HTN-102050-0007-A
Supercedes HYTEC-TN-GLAST-10
4/12/2000

GLAST Tray Dynamic Response Trend Studies

Franz Biehl
September 13, 1999

Abstract

Finite element models of the present GLAST tray design were examined in an effort to identify an optimum configuration from the standpoint of minimum displacement excursions during random vibration excitation. It was found that the present design using composite face sheets offers a reasonable random response displacement.

DESIGN ENGINEERING
ADVANCED COMPOSITE APPLICATIONS
ULTRA-STABLE PLATFORMS

110 EASTGATE DR.
LOS ALAMOS, NM 87544

PHONE 505 661•3000
FAX 505 662•5179
WWW.HYTECINC.COM

Revision Log

Revision	Date	Author	Summary of Revisions/Comments
OI	September 13, 1999	F. Biehl	Initial release.
A	April 12, 2000	F. Biehl	Updated document number, added Revision log

Table of Contents

1. Summary

This report presents a summary of calculated trend study results for standard and superglast tray designs. The results are presented in the form of resonant frequency and random response amplitudes as functions of tray design parameters. Design parameters are considered as a means to affect the stiffness of either the closeout frame, core, or face sheet. The design parameters are then portrayed as factors on the contributing structural stiffness.

Two finite element models simulating the tray design are examined. Both models simulate the details of the actual closeout frame design and both treat the honeycomb core with solid elements. The first model is designated as the "payload model" where the honeycomb face sheets are separated as distinct shell elements from the remaining payload structure that consists of epoxy, converter, bias circuit, and detector layers. The payload is represented by a single layer of finite shell elements where the membrane stiffness simulates the effective payload in-plane or membrane stiffness. All of the trend results reported are derived from this payload model.

A second model differs from the first in the treatment of the face sheet plus payload simulation. With this model the face sheet plus converter and bias circuit are combined in one composite shell element layer and the detectors plus detector bonds are simulated as separate finite element members. This representation is designated as the "detector model" and is included in the report to show that careful consideration should be given to the bond configuration attaching the individual detectors to the tray surface.

2. Baseline Configuration Description

2.1 General baseline assembly

The baseline model (approximately 38 cm square) consists of an aluminum closeout frame, aluminum honeycomb core, graphite/epoxy composite face sheets, and top and bottom payloads. The payloads consist of detector elements, bias circuit panels, converters, and epoxy bond material between the various layers. Trend study effects are achieved by changing face sheet laminate, core, and/or closeout frame properties. The difference between the standard GLAST tray and the super GLAST tray is the thickness of the lead converter. For the normal tray the lead thickness is 0.2mm while for the super tray the thickness is 1.4mm.

2.2 Baseline closeout frame and honeycomb core

Figure 1 shows several photographs of the first GLAST tray frame design at approximately 32 cm square. The new configuration discussed in this report is approximately 38 cm square as detailed in HYTEC drawing HYT-GLS-0010 (design details are essentially the same as the original). The frame material is 6061-T6 aluminum. The core is fabricated from HEXCEL[1] honeycomb core designated as aluminum 3/8in-5052-0.002in-3lb/ft^3. Frame and core properties are given in Table 1.

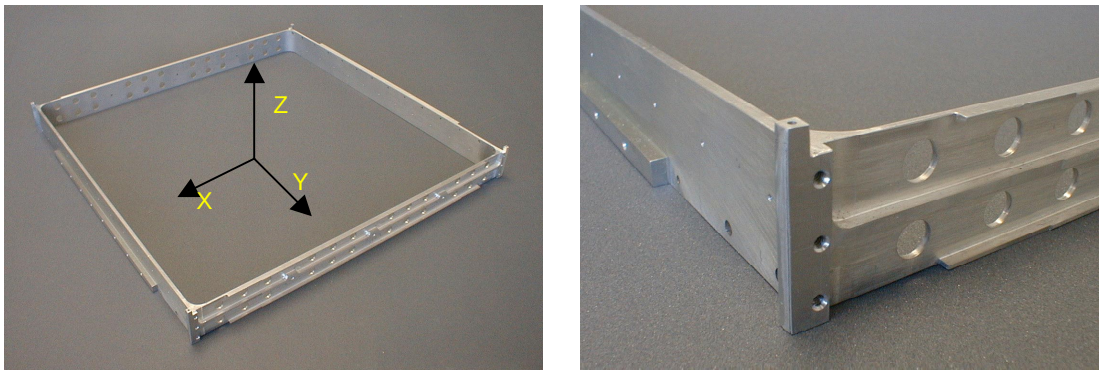

Figure 1: GLAST tray closeout frame (32 cm frame shown – actual frame is approximately 38 cm).

Item	Material	Cell width	Web thick.	Density	Modulus E_x or E_z*		Shear modulus G_{xz}		Shear modulus G_{yz}	
		in	in	Kg/m^3	ksi	GPa	ksi	GPa	ksi	GPa
Frame	6061-T6	NA	NA	2700	10e3	69				
Core	5052	3/8	.002	48	70.0	0.483	43.0	0.297	21.2	0.146

* E_x applies to the frame while E_z is the core compression stiffness

Table 1: Baseline closeout frame and core properties.

2.3 Baseline face sheet plus payload

Figure 2 is a schematic sketch of the baseline bottom face sheet plus payload configuration. Table 2 presents the material descriptions and baseline thickness dimensions for both the top and bottom payload elements plus face sheet.

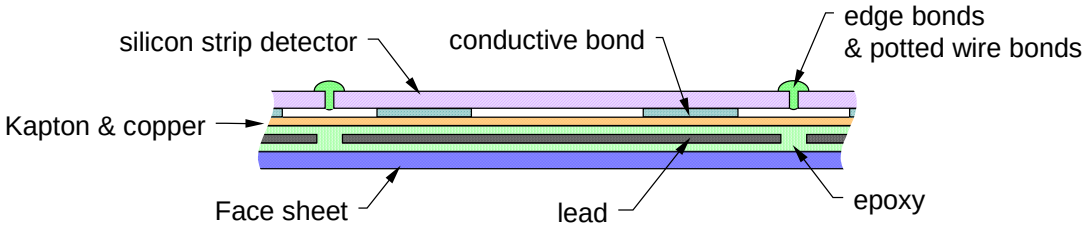

Figure 2: Cross-section of bottom payload configuration (the top payload has no lead converters).

Layer Description	Modulus of Elasticity (GPa)	Density (kg/m^3)	Tray Material Layer			
			top		bottom	
			material	thickness (mm)	material	thickness (mm)
Detector	131.0	2330	Silicon	0.4	Silicon	0.4
Edge bond	3.0	1800	Epoxy (1)		Epoxy(1)	
Detector bond	3.0	1800	Epoxy	0.075	Epoxy	0.075
Bias circuit	17.3	2265	Kapton and copper	0.152	Kapton and copper	0.152
Bias circuit bond	3.0	1800	Epoxy	0.075	Epoxy	0.075
Converter	13.8	11340	-	-	Lead	0.2 (2)
Converter bond	3.0	1800	-	-	Epoxy	0.075
Face sheet	90	1700	Grp/epxy	0.318	Grp/epxy	0.318

(1) in ladder direction only
(2) superglast lead converter is 1.4mm thick

Table 2: Baseline tray material description.

3. Finite Element Model (FEM) Description

3.1 Baseline model

The COSMOS[1] finite element code was used to construct and process the finite element models discussed in this document. The baseline FEM consists of a simulated closeout frame using shell and solid finite elements, simulated honeycomb core using solid elements, simulated face sheets using shell elements, and simulated payloads using shell elements. Each face sheet is assumed to be a six-ply laminate with a [0,+60,-60,-60,+60,0] layup. This "balanced" arrangement leads to a quasi-isotropic laminate. Calculated effective in-plane and bending stiffness properties are detailed in Appendix A. Payloads are simulated by thin (0.001mm) shell elements that equate the individual layer in-plane stiffness to a composite single equivalent layer in-plane stiffness. The equivalent stiffness model is constructed as shown in Appendix B. Closeout frame and core finite element meshes are displayed in Figure 3.

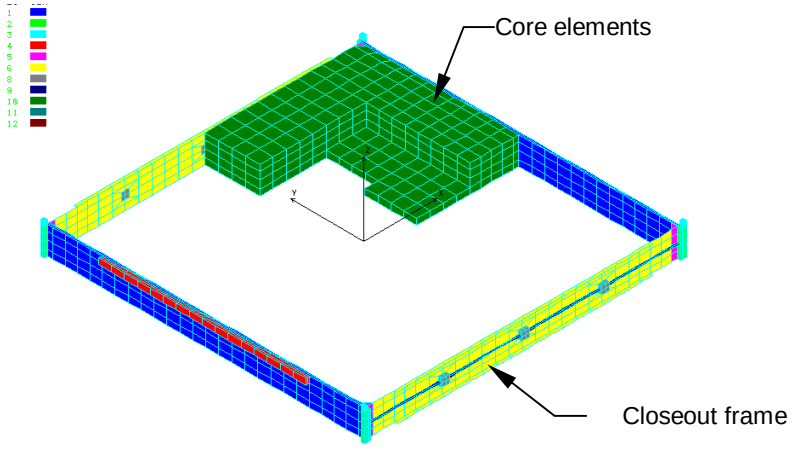

Figure 3: Tray FEM model showing closeout frame and honeycomb cell elements and including coordinate system.

3.2 Baseline FEM mass distribution

The baseline FEM mass distribution for the normal GLAST and superglast GLAST trays are listed in Table 3. Model dimensions and densities are given in Tables 1 and 2.

Component	Normal tray mass (kg)	Superglast tray mass (kg)
Closeout frame	0.290	0.290
Honeycomb core	0.195	0.195
Top face sheet	0.081	0.081
Bottom face sheet	0.081	0.081
Top payload	0.236	0.236
Bottom payload	0.565	2.541
Total	**1.448**	**3.424**

Table 3: Finite element model mass distribution

4. Calculated Results (payload model)

4.1 Variation in core stiffness with baseline face sheet

In this study it is assumed that the core properties (*Ez*, *Gxz*, *Gyz*, and density) can be multiplied by a constant to represent a variation in core stiffness (baseline is 1.0). The computed results are listed in Table 4 and shown in Figure 2.

Core factor	Standard tray		Superglast tray	
	Mass (kg)	Frequency (Hz)	Mass (kg)	Frequency (Hz)
0.25	1.302	658	3.278	390
0.4			3.307	444
0.5	1.350	771	3.326	468
0.75	1.399	818	3.375	507
1.0	1.448	840	3.424	529
1.25	1.497	849	3.472	543
1.5	1.545	851	3.521	552
1.75			3.570	558
2.0	1.643	844	3.618	562
2.5			3.716	565

Table 4: Calculated mass and first mode frequency for variation in core stiffness with fixed baseline face sheet (payload model).

In generating the results appearing in Table 4 and Figures 4 and 5 it was assumed that the core properties listed in Table 1 could be multiplied by the core factor constants to obtain revised properties. An examination of actual honeycomb property data indicates that stiffness and mass density values are not necessarily linearly related. Thus, these results are somewhat arbitrary with respect to the variation of all stiffness properties. As a check on this approach, a calculation using a "light" core that was used in the Tray 1^2 assembly is plotted in Figure 4. The relative stiffness ratio in core shear (Gxz) was used as the core

factor parameter. Inspection of Figure 4 shows that the present core factor approach is representative of other core configurations.

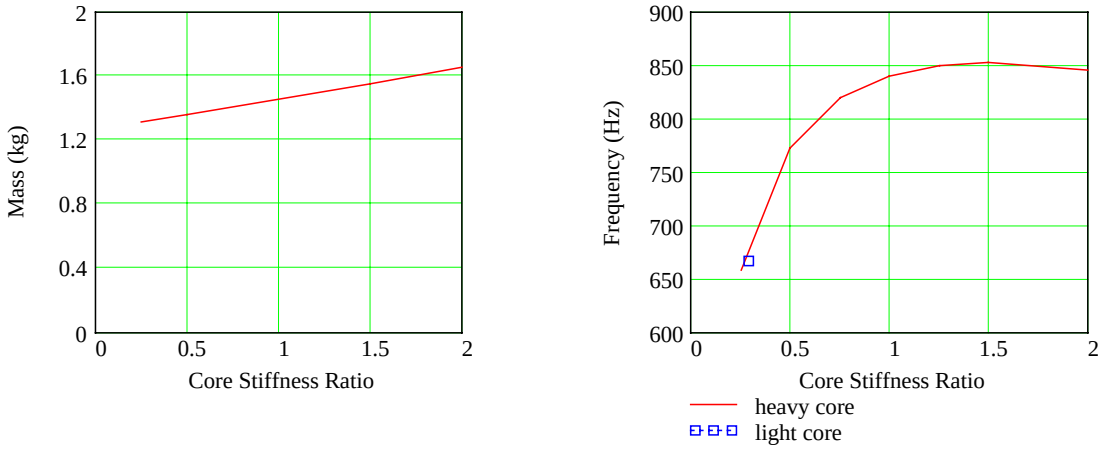

Figure 4: Tray mass and first mode frequency as function of core stiffness with fixed face sheet (standard tray).

The right hand plot in Figure 4 shows an additional result denoted by "light core" that had been obtained by using an actual more flexible core (3/8in-5052-0.0007in-1.0 lb/ft^3)^3.

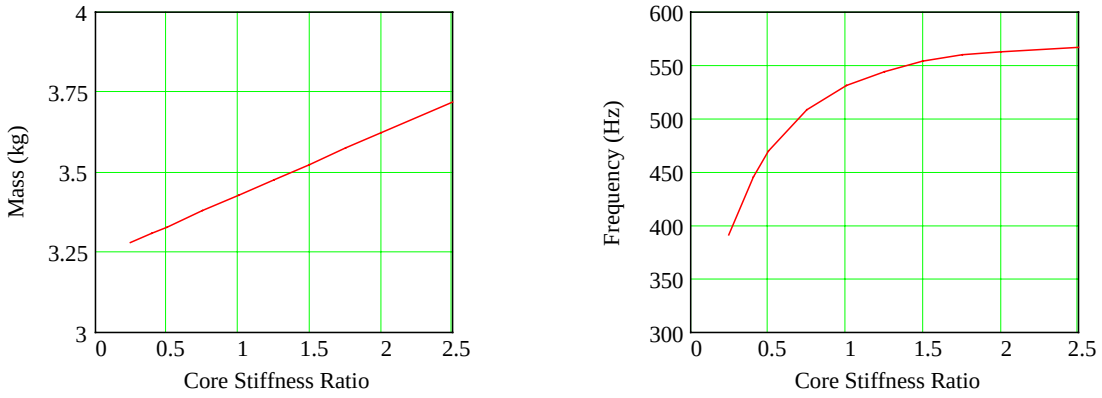

Figure 5: Tray mass and first mode frequency as function of core stiffness with fixed face sheet (superglast tray).

4.2 Variation in face sheet stiffness

The variation in first mode frequency with constant baseline core properties while changing the face sheet stiffness modulus (*Ex*, *Ey* and *Gxy* holding *Nuxy* constant) is listed in Table 5 and depicted in Figure 6. To obtain these results it was assumed that for the standard tray the face sheet thickness and density would remain constant implying that a material could be found that changed stiffness properties only.

Face sheet factor	Standard tray		Superglast tray	
	Mass (kg)	Frequency (Hz)	Mass (kg)	Frequency (Hz)
0.25	1.448	655	3.343	481
0.5	1.448	739	3.383	509
0.75	1.448	796		
1.0	1.448	840	3.424	529
1.25	1.448	875	3.464	545
1.5	1.448	905	3.505	558
2.00	1.448	953	3.586	578
2.50	1.448	989		
4.0			3.910	617

Table 5: First mode frequency as a function of face sheet factor (core factor fixed at 1.0)

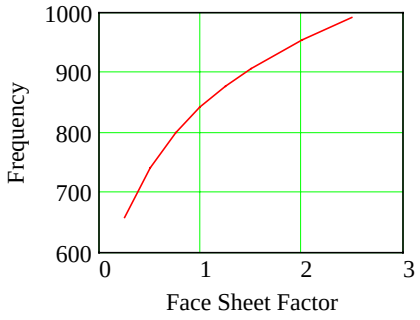

Figure 6: Tray first mode frequency as a function of face sheet factor (standard tray).

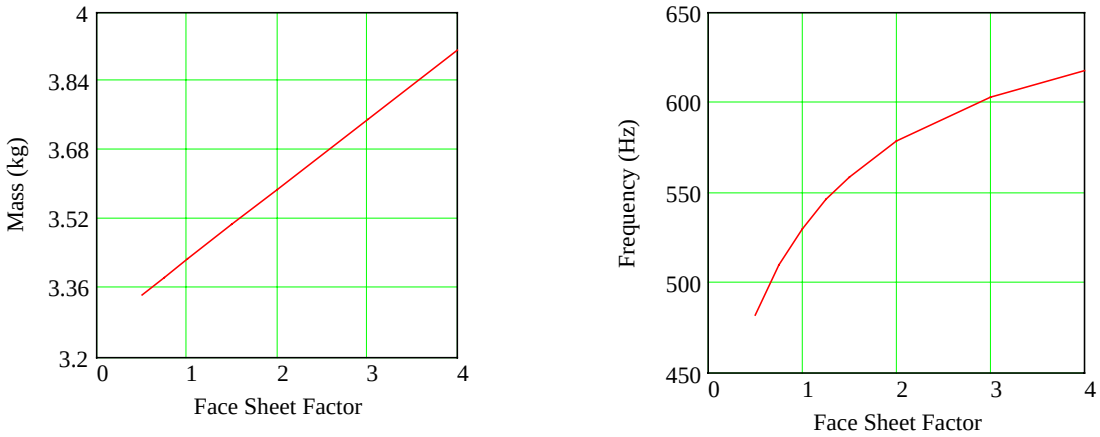

Figure 7: Tray first mode frequency as a function of face sheet factor (superglast tray).

4.3 Simultaneous variation in core and face sheet stiffness

4.3.1 Standard tray

The influence on first mode frequency and mass by variations in core and face sheet stiffness factor is listed in Table 6 and graphically displayed in the Figures 8 through 10. Core mass properties changed while the face sheet density and thickness were held constant.

Face sheet factor	Core factor (tabulated frequency (Hz))					
	0.5	**0.75**	**1.0**	**1.25**	**1.5**	**2.0**
Mass(kg)	1.350	1.399	1.448	1.497	1.545	1.643
0.5	694	727	739	743	741	730
0.75	738	779	796	802	803	794
1.00	771	818	840	849	851	844
1.25	797	850	875	887	890	886
1.50	818	876	905	919	924	922
2.0	851	918	952	971	979	978
2.50	876	950	989	1011	1021	1026

Table 6: First mode frequency as a function of variation in face sheet factor and core factor (standard tray).

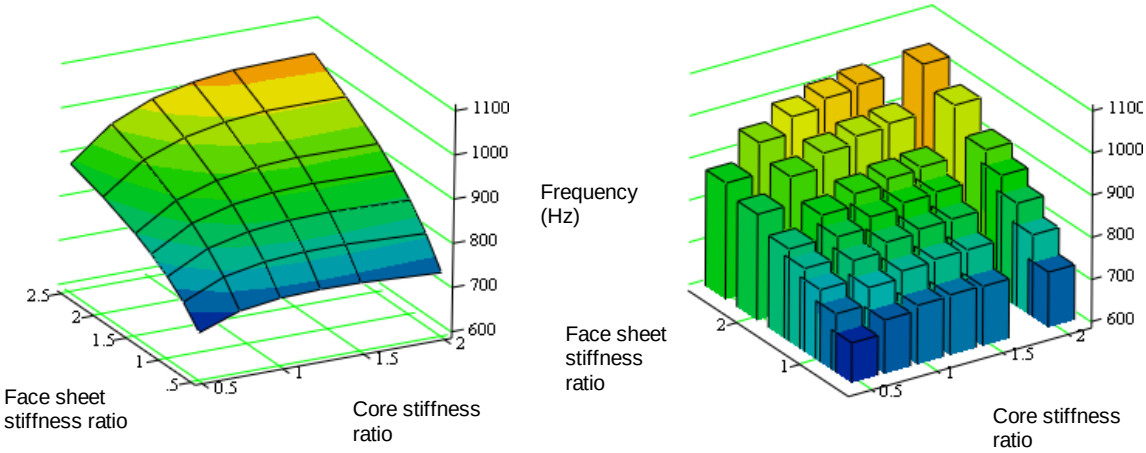

Figure 8: Plots of frequency (vertical axis) versus core factor (right axis) and face sheet factor (left axis).

Inspection of Figure 8 shows that there is little to gain in terms of increased first mode frequency by increasing the core factor; whereas, modest improvements can be gained with increasing face sheet factor. Subsequent results of response to random base motion will show that there is little incentive to increase the first mode frequency in order to achieve lesser relative displacement between the panel midpoint and the support frame.

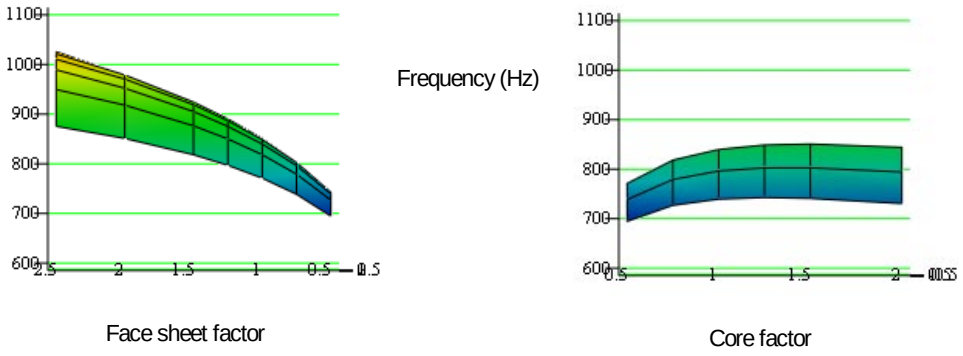

Figure 9: Left view is frequency versus face sheet factor and right view is frequency versus core factor.

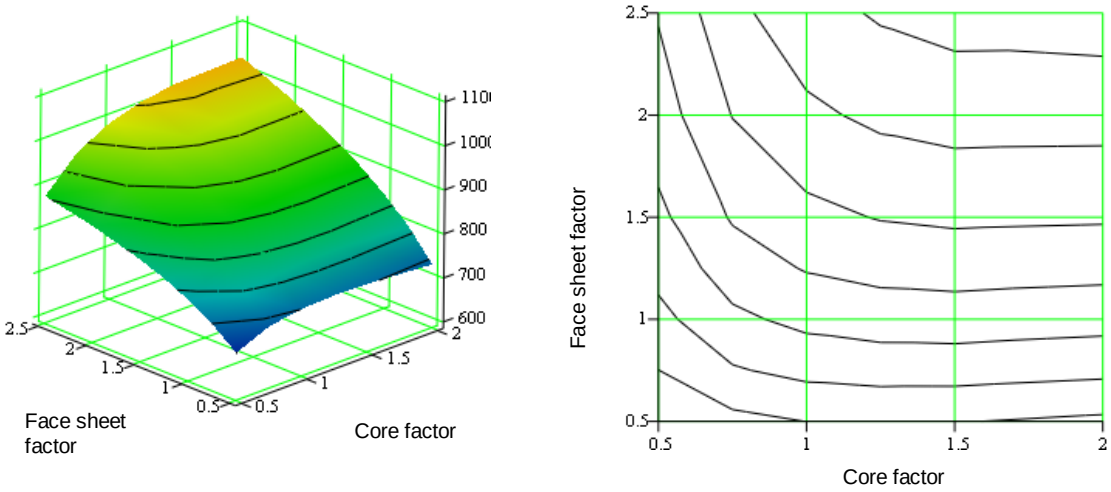

Figure 10: Contour plots of constant frequency, right plot is view from top side.

4.3.2 Superglast tray

The influence on first mode frequency by variations in core and face sheet stiffness factor is listed in Table 7 and graphically displayed in the Figures 11 through 13. The total mass as functions of face sheet factor and core factor is listed in Table 8.

Face sheet factor	Core factor (tabulated frequency (Hz))							
	0.5	**0.75**	**1.0**	**1.25**	**1.5**	**1.75**	**2.0**	**2.5**
0.5	435	465	481	491	497	501	503	504
0.75	455	489	509	521	528	533	537	538
1.0	469	507	529	543	552	558	562	565
1.25	479	521	545	561	571	578	583	587
1.5	487	532	558	575	587	595	600	606
2.0	498	548	578	598	611	621	627	633
4.0	518	578	617	644	664	678	689	704

Table 7: First mode frequency as a function of face sheet factor and core factor (superglast tray).

Face sheet factor	Core factor (tabulated mass (kg))							
	0.5	0.75	1.0	1.25	1.5	1.75	2.0	2.5
0.5	3.245	3.294	3.343	3.391	3.440	3.489	3.537	3.636
0.75	3.286	3.334	3.383	3.432	3.481	3.529	3.578	3.675
1.0	3.326	3.375	3.424	3.472	3.521	3.570	3.618	3.716
1.25	3.367	3.415	3.464	3.513	3.562	3.610	3.659	3.756
1.5	3.407	3.456	3.505	3.553	3.607	3.651	3.699	3.797
2.0	3.488	3.537	3.586	3.634	3.683	3.732	3.781	3.878
4.0	3.813	3.861	3.910	3.959	4.007	4.056	4.105	4.202

Table 8: Tray mass as a function of face sheet factor and core factor (superglast tray)

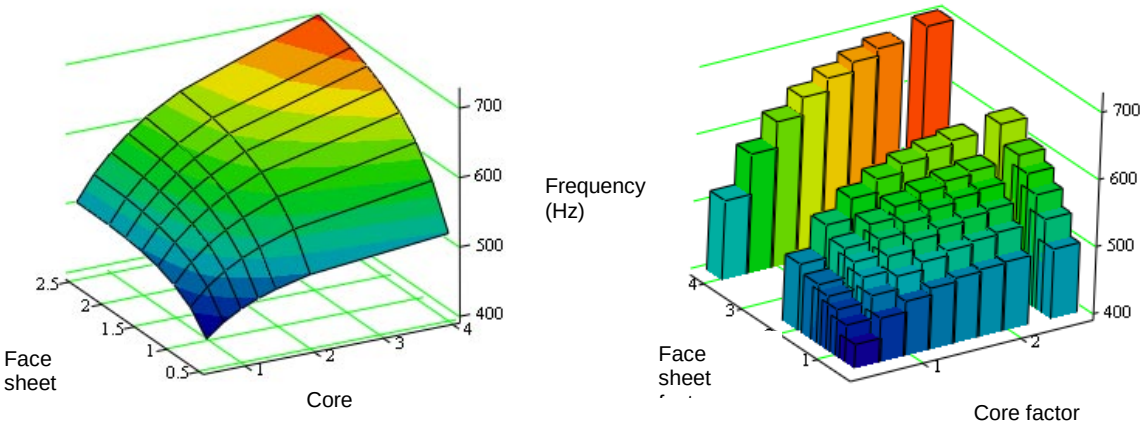

Figure 11: Plots of frequency (vertical axis) versus core factor (right axis) and face sheet factor (left axis) (superglast tray).

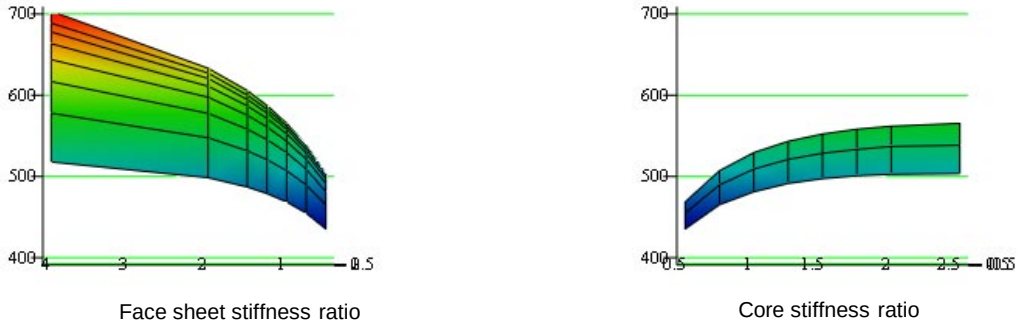

Figure 12: Left view is frequency versus face sheet factor and right view is frequency versus core factor (superglast tray).

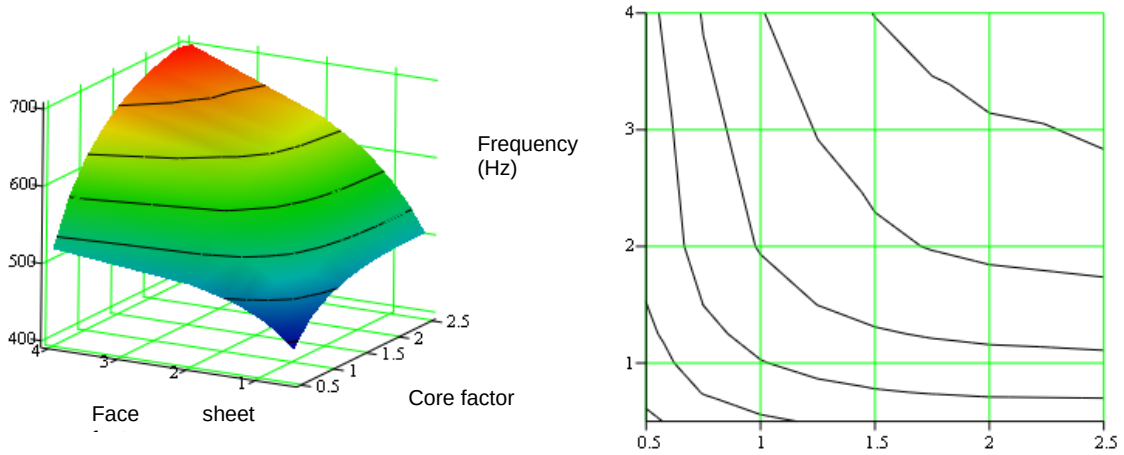

Figure 13: Contour plots of constant frequency, right plot is view from top side.

4.4 Effect of closeout frame stiffness

The effect of variation in the closeout frame stiffness (defined by *Ex*, *Gxy*, and *Nuxy*) on first mode frequency using fixed baseline face sheet and core properties is listed in Table 7 and displayed in Figure 9. These results show that the support frame stiffness has little influence on the first mode reaching about + or – 3% at the extremes values of stiffness. Again it assumed that the stiffness is achieved without a change in dimensions or density.

Closeout frame factor	First mode frequency (Hz)	
	Standard	Superglast
0.5	807	508
1.0 (baseline)	840	529
1.5	854	539
2.00	862	544

Table 9: First mode frequency as a function of closeout frame factor (core and face sheets at fixed baseline properties).

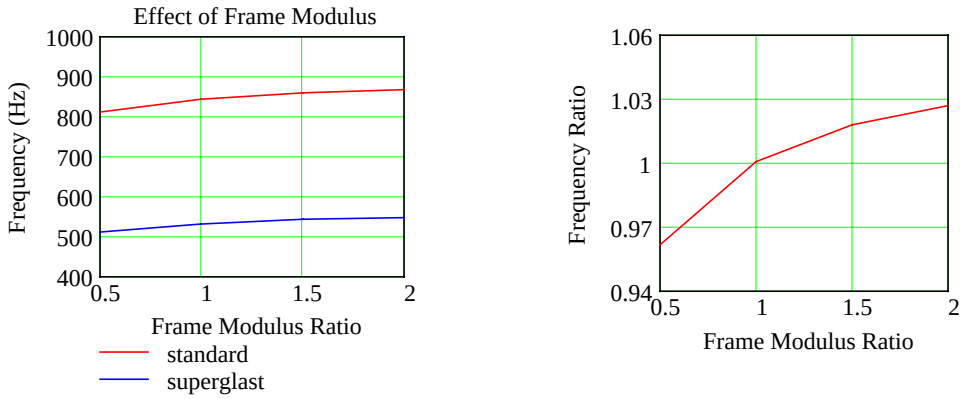

Figure 14: Effect of closeout frame stiffness on first mode frequency. Plot on right shows about a 3% change for half or double stiffness ratios (applies to both the standard and superglast trays).

4.5 Effect of face sheet laminate orientation

The effect of face sheet lamination direction with respect to the first mode frequency is presented in Table 8. As indicated by the listed resulting modulus, the face sheets are orthotropic (*Ex* is not equal to *Ey*). Examination of Table 8 shows that there is not a substantial effect due to the variation in face sheet configuration. Each lamina thickness is the same as in the baseline case, the difference occurs in the lamina sheet directions. The baseline case is included for comparison purposes. The face sheet *0* degree angle (or direction) is along the model system *X* direction. There appears to be a slight advantage to orienting most of the lamina along the *Y* direction.

Core direction	Face sheet definition			Frequency (Hz)	
	Lamination angles (deg)	Ex (GPa)	Ey (GPa)	Standard	Superglast
X	0/90/90/90/90/0	90	174	828	521
X	90/0/0/0/0/90	174	90	795	503
Y	0/90/90/90/90/0	90	174	828	522
Y	90/0/0/0/0/90	174	90	847	534
X	baseline	90	90	840	529
X	0/90/0/90	110	110	775	487
X	0/90/0/0	192	37	739	467
X	90/0/90/90	37	192	777	489

Table 10: First mode frequency as a function of core direction and face sheet lamina direction.

5. Response to Random Vibration

5.1 White noise excitation to closeout frame (base support excitation)

Tray midpoint response to a closeout frame random vibration excitation can be calculated by the closed-form expression

$$R_{RMS} = \sqrt{\frac{8\,Sf\,Q}{\pi^7\,fn^3}}, \tag{1}$$

where R_{RMS} (m) is the RMS response, Sf $[(m/s^2)^2/Hz]$ the input white noise spectrum, Q the quality factor (assumed 40), and fn (Hz) the resonant frequency. Figure 15 shows the calculated results where the left axis is the core ratio and the right axis the face sheet ratio.

5.2 RMS Response

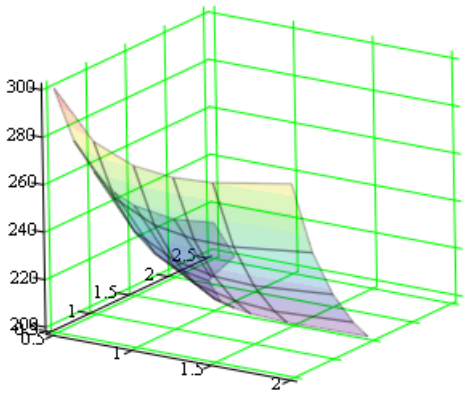

x

(cf , fsf , RMSf)

Figure 15: Tray midpoint response to closeout frame flat random acceleration spectrum (0.16 g^2/Hz).

RMS Response Function of Core and Face Sheet

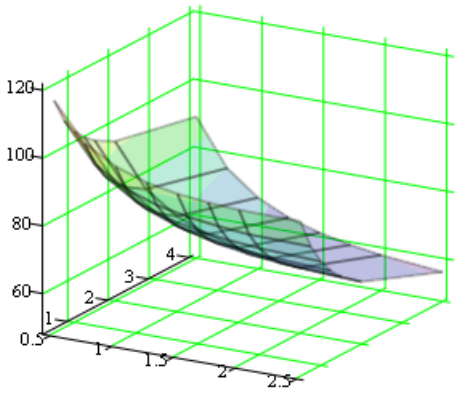

Figure 16: Tray midpoint response to closeout frame flat random acceleration spectrum (0.16 g^2/Hz) (superglast tray).

5.2 Probability factor applied

The derivation of a factor of 5.2 applied to the RMS response is presented in Reference 2. Results of the applied factor on the single displacement for each tray midpoint is presented in Figure 17.

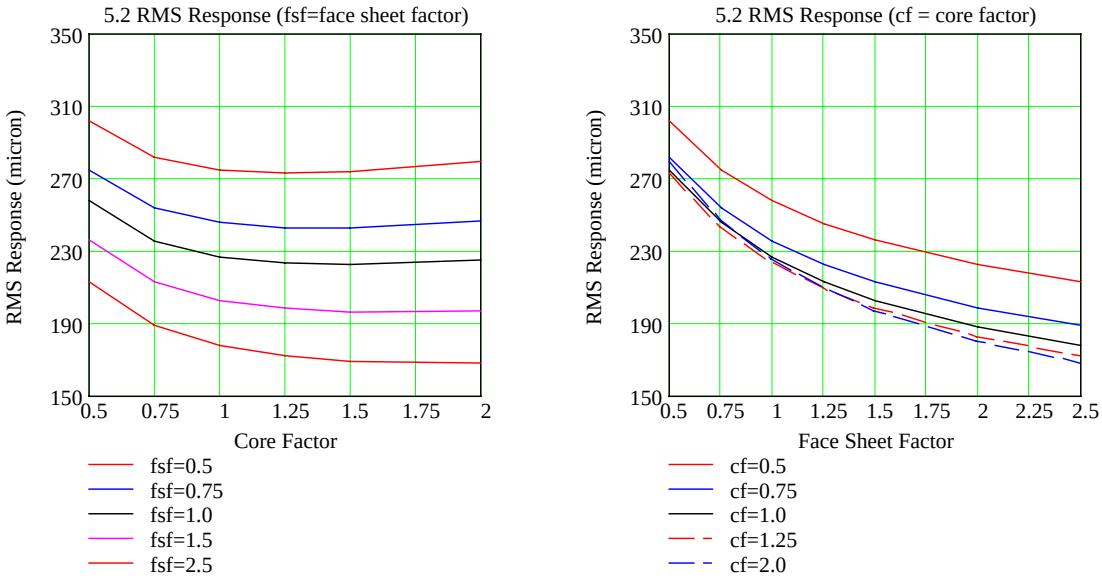

Figure 17: Tray midpoint response to random input with applied 5.2 factor as a function of core factor and face sheet factor.

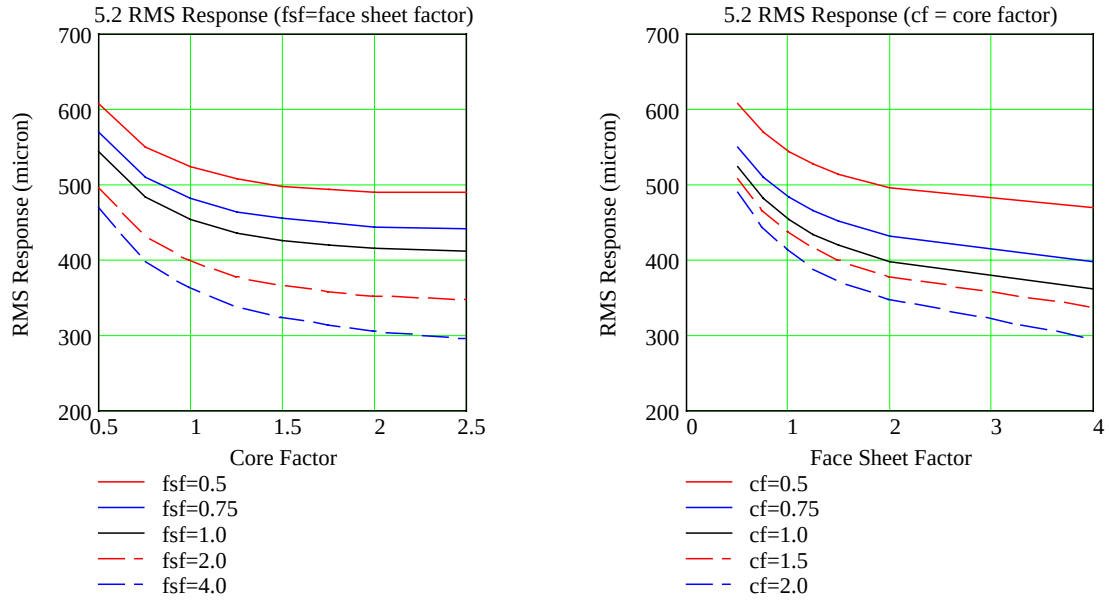

Figure 18: Tray midpoint response to random input with applied 5.2 factor as a function of core factor and face sheet factor (superglast tray).

6. Detector Model

6.1 Individual detector vibration response

The FEM model representation described in the previous sections treat the detectors as “layered” with the bias, epoxy, and lead as a single composite layered shell

finite element. This approach constrains the individual detector vibration response to be equivalent to the payload-face sheet composite assembly. In a present design, the detectors are attached to the bias panel via three individual squares of thin epoxy "pads" covering somewhere around 10 to 20% of the each detector area. This arrangement leads to individual detector vibration modes that tend to appear somewhat independent of the overall tray panel modes. In addition, detector vibration response could tend to increase the probability of contact between trays.

6.2 Individual detector modes

A closed form calculation of an individual detector on simple edge supports on all four sides shows a resonant frequency of 316 Hz. A FEM of a single detector supported at three epoxy pads indicates a first "flapping" mode (edge displacement rather than panel bending) at 420 Hz while a model with four support pads is about 890 Hz. Individual detector frequencies will be shifted when attached to the tray surfaces due to the change in support boundary conditions. When individual detectors are assembled in a "ladder" configuration, the addition of more support constraints (such as "potting" between detectors) will result in revised modal frequencies.

6.3 Discrete detector members

An alternative FEM that represents the detectors as discrete structural members has been constructed. The model incorporates shell finite elements for the detectors, solid finite elements simulating the pads connecting the detector to the tray surfaces, and shell elements simulating the edge bonding potting material between detector segments. This model permits an examination of the response of individual detector segments to the vibration input conditions described in previous sections of this report. The first tray assembly mode for an assumed four pad detector support design is displayed in Figures 19 and 20. Figure 19 plots the upper and lower detectors while Figure 20 plots only the lower detectors. Each Figure shows a substantial contribution from detector edge bending displacement. The second calculated vibration mode displayed in Figure 21 is the first among many detector displacement mode shapes wherein the panel displacement is nearly zero.

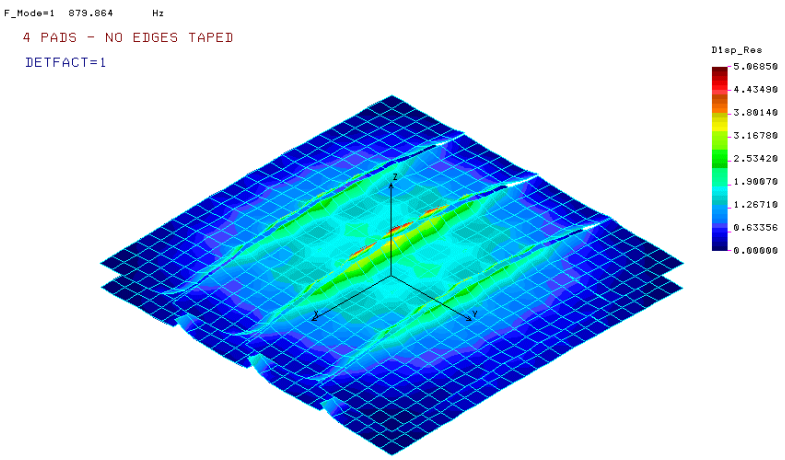

Figure 19: First mode shape of detector model showing substantial displacement by detectors (detectors only).

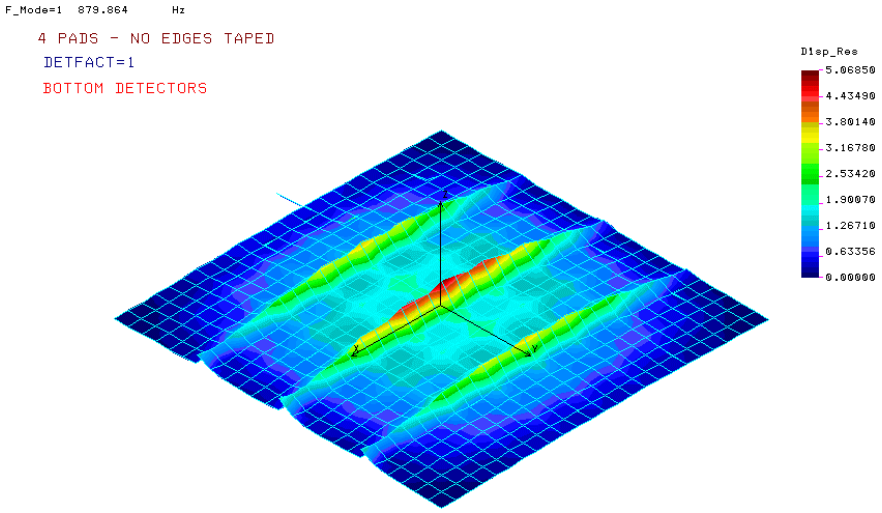

Figure 20: First mode of detector model showing array bottom detectors only (X is ladder direction).

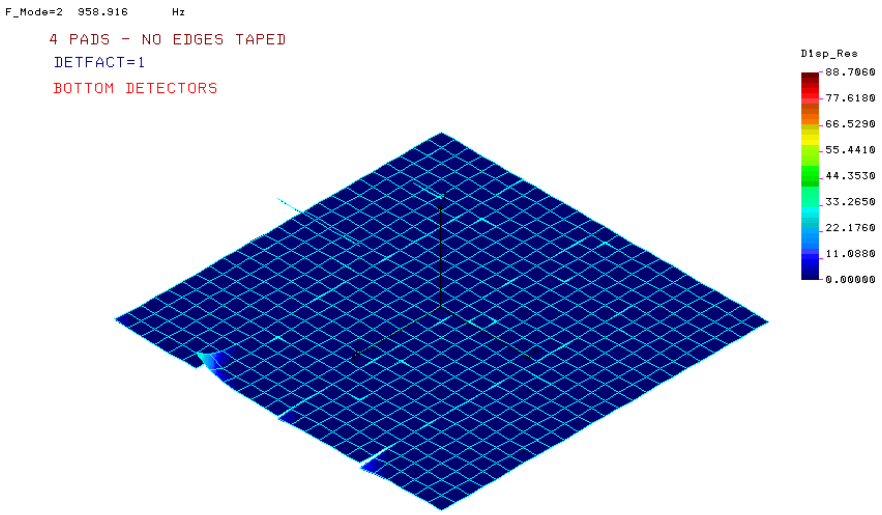

Figure 21: Second mode shape for detector model showing a representative detector edge bending displacement.

6.4 Comparison with payload model

The first panel bending mode frequency (876 Hz) for the alternative model is higher than the first mode for the standard tray payload model reported in previous sections (840 Hz). A three-pad support configuration model results in a first mode frequency of 837 Hz. For this three-pad design a detector stiffness factor is used to ensure detector edge modes are above the tray first panel bending mode. This factor is applied to increase the detector bending stiffness while maintaining the detector

membrane stiffness. The close agreement in frequency (837 versus 840 Hz) between the three-pad configuration and the standard tray model suggests that either model is representative of the tray response. This can also be extended to the four-pad configuration. In order to ensure that the trend effects reported for the payload model can be applied to the detector model, a representative trend performance is listed in Tables 11 and 12.

Core direction	Face sheet definition			Frequency (Hz)	
	Lamination angles (deg)	Ex (GPa)	Ey (GPa)	Payload model	Detector model
X	0/90/90/90/90/0	90	174	828	837
X	90/0/0/0/0/90	174	90	795	842
Y	0/90/90/90/90/0	90	174	828	831
Y	90/0/0/0/0/90	174	90	847	805
X	baseline	90	90	840	876
X	0/90/0/90	110	110	775	779
X	0/90/0/0	192	37	739	753
X	90/0/90/90	37	192	777	792

Table 11: Comparison of trends between the standard payload tray model and the detector standard tray model.

Face sheet factor	Superglast payload model		Superglast detector model	
	Mass (kg)	Frequency (Hz)	Mass (kg)	Frequency (Hz)
0.25	3.343	481	3.203	480
0.5	3.383	509	3.383	523
1.0	3.424	529	3.322	573
1.25	3.464	545	3.362	590
1.5	3.505	558	3.403	603
2.00	3.586	578	3.482	624
4.0	3.910	617	3.801	666

Table 12: Comparison of trends between the superglast payload tray model and the detector superglast tray model.

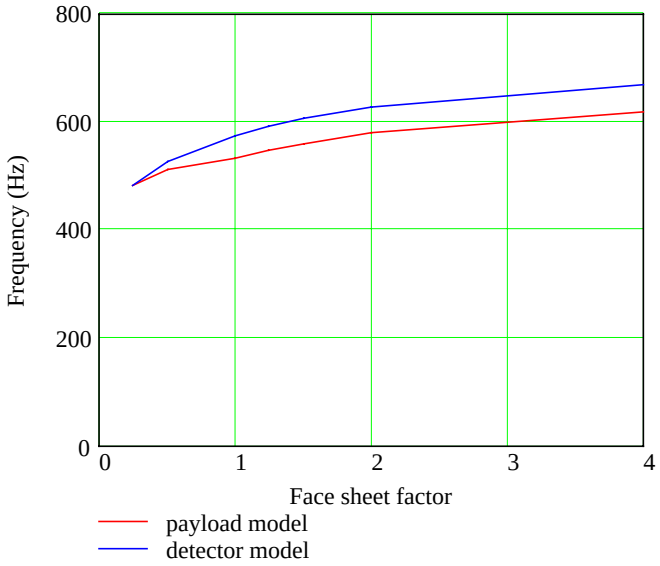

Figure 22: Plot of frequency as a function of face sheet factor comparing payload model with detector model (superglast tray).

7. Conclusions

The calculated results shown in this report support the conclusion that a standard tray is about at the optimum design while the superglast tray design would profit from further design modifications.

8. References

1. COSMOS/M 2.0 for Windows Platforms, Structural Research and Analysis Corporation, Los Angeles, CA.
2. Franz Biehl, Eric Ponslet *Beam Test Trays 1999- Dynamic Predictions for Trays Tested at NASA/GSFC in April 99*, HYTEC Inc., Los Alamos, NM document HYTEC-TN-GLAST-06, May 1999.
3. HEXCEL document TSB 120, *Mechanical Properties of Hexcel Honeycomb Materials.*
4. Robert M. Jones, Mechanics of Composite Materials, Hemisphere Publishing Corporation.

9. Appendix A: Calculation of face sheet laminate properties

The derivation of face sheet laminate material properties is presented in this Appendix. The formulas used are presented in Reference 4. The in-plane stress-strain relation for a single layer lamina is given by

$$\sigma = [Q]\varepsilon, \textit{ where} \tag{A1}$$

$$[Q] = \begin{bmatrix} \dfrac{Ex}{1-\nu xy\,\nu yx} & \dfrac{\nu xy\,Ey}{1-\nu xy\,\nu yx} & 0 \\ \dfrac{\nu xy\,Ey}{1-\nu xy\,\nu yx} & \dfrac{Ey}{1-\nu xy\,\nu yx} & 0 \\ 0 & 0 & Gxy \end{bmatrix}, \tag{A2}$$

where E, ν, and G denote elastic modulus, Poisson ratio, and shear modulus, respectively. The stress relation can be rotated to represent the fiber direction (or Ex direction) to another angle (θ) by

$$[Q(\theta)] = [T^{-1}][Q][T^{-1}]^T \textit{ , where} \tag{A3}$$

$$[T] = \begin{bmatrix} \cos^2\theta & \sin^2\theta & 2\sin\theta\cos\theta \\ \sin^2\theta & \cos^2\theta & -2\sin\theta\cos\theta \\ -\sin\theta\cos\theta & \sin\theta\cos\theta & \cos^2\theta - \sin^2\theta \end{bmatrix}. \tag{A4}$$

The Q matrix is found for each individual lamina (layer) comprising the composite and the subsequent in-plane stiffness properties are derived from the composite stress-strain matrix. The composite in-plane matrix is found from

$$Qc = \frac{1}{tk}\sum_{k=1}^{n} Q_k\left(z_k - z_{k+1}\right), \tag{A5}$$

where k is a subscript denoting each layer, z is the distance of the layer boundaries from the middle surface, and tk is the total composite thickness. Elastic properties are then extracted from the composite Qc matrix by

$$\nu xy = \frac{Qc_{1,2}}{Qc_{2,2}}, \quad \nu yx = \frac{Qc_{1,2}}{Qc_{1,1}}, \quad Exx = \frac{Qc_{1,1}}{1-\nu xy\,\nu yx}, \quad Eyy = \frac{Qc_{2,2}}{1-\nu xy\,\nu yx}, \quad Gxy = Qc_{3,3}. \tag{A6}$$

Face sheet properties can be entered by layers or by a single layer in the finite element model. It was desired that the isotropic in-plane modulus be equal to 90Mpa, that six layers at 0, 60, -60, -60, 60, and 0 degrees be used, and that the total thickness be 0.318mm. Furthermore, it was estimated that each layer would consist of 60% volume fraction graphite fibers with an epoxy binder. The lamina properties are calculated from

$$Ex = Ef\,Vf + Em\,Vm \tag{A7}$$

$$Ey = \frac{Em}{Vm + Vf\,\frac{Em}{Ef}} \tag{A8}$$

$$vxy = Vm\,vm + Vf\,vf \tag{A9}$$

$$vyx = vxy\,\frac{Ey}{Ex} \tag{A10}$$

$$Gf = \frac{Ef}{2(1+vf)} \qquad Gm = \frac{Em}{2(1+vm)} \tag{A11}$$

$$Gxy = \frac{Gm\,Gf}{Vm\,Gf + Vf\,Gm} \tag{A12}$$

where
Ef = fiber modulus (426.417GPa assumed)
Em = matrix (epoxy) modulus (2.8GPa assumed)
Vf = fiber volume fraction (0.6 assumed)
Vm = matrix volume fraction (1.0-Vf)
vf = fiber Poisson ratio (0.24 assumed)
vm = matrix Poisson ratio (0.35 assumed)

Calculated composite properties using (A7) through (A12) when substituted into (A1) through (A7) are listed in Table 13 as quasi-isotropic face sheet elastic constants. As discussed earlier, orthotropic composites were also examined as candidate face sheet panels. Elastic constants for an arrangement of 0, 90, -90, -90, 90, and 0 (note that 90 and –90 degree have the same effect) degree layers are listed as orthotropic properties in Table 13.

Property	Quasi-isotropic	Orthotropic
	0/60/-60/-60/60/0	**0/90/-90/-90/90/0**
Exx (Gpa)	90.00	90.45
Eyy (Gpa)	90.00	173.96
vxy	0.329	0.022
vyx	0.329	0.011
Gxy (Gpa)	33.85	2.57

Table 13: Calculated composite properties used in face sheet simulation.

10. Appendix B: Payload Stiffness and Mass

10.1 Equivalent stiffness model

To calculate the effective modulus-thickness product (*Et*) for each face sheet/payload combination, a series of equivalent simple spring models are sketched that

represent a particular composite payload. For example, Figure 23 represents a single section of the tray 1 bottom composite payload (face sheet + payload).

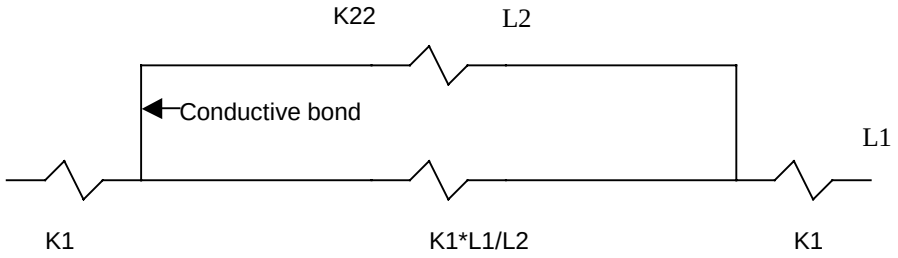

Figure 23: Stiffness schematic of tray 1 bottom composite payload (one detector segment).

In Figure 12 the parameter *K1* represents the stiffness between detector sectors. For the "ladder" direction (*X* in the FEM) *K1* includes the stiffness contribution from the potting material between detector segments at a gap length denoted by L1. In the "non ladder" direction (*Y* in the FEM), *K1* does not include the potting material stiffness. *K22* is the detector spring stiffness and for this case is effective only between the start and end of the conductive bond connectors as there is no potting material between adjoining detector segments. Equivalent spring elements are determined from modulus-thickness products for the various layers included in the payload-face sheet composite. The face sheet may or may not be isotropic; therefore, the face sheet requires an additional subscript denoting the modulus direction. The required definitions used in the composite model are

$$\begin{aligned} ET_d &= E_d tk_d \\ ET_b &= E_b tk_b \\ ET_c &= E_c tk_c \\ ET_{fsX} &= E_{fsX} tk_{fs} \\ ET_{fsY} &= E_{fsY} tk_{fs} \\ ET_{bd} &= E_{bd} tk_{bd} \\ ET_{b\,\mathrm{det}} &= E_{bd} tk_d \end{aligned} \qquad \text{(B1)}$$

where *E* is the modulus, *tk* the thickness, and *ET* the modulus-thickness product. The subscripts *d, b, c, fsX, fsY,* and *bd* denote the detector, bias board, converter, face sheet *X* direction, face sheet *Y* direction, and bond material; respectively.

10.2 Composite ET in non ladder direction (*Y*)

The *Y* direction (non ladder) equivalent composite *ET* product is computed as follows

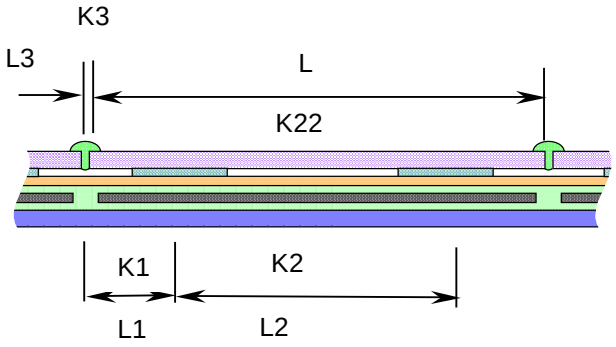

$$K1 = \frac{W}{L1}\left(ET_{fsY} + Et_b + ET_c\right) \tag{B2}$$

$$K22 = \frac{W}{L2} ET_d \tag{B3}$$

$$K2 = \frac{L1}{L2} K1 + K22 \tag{B3}$$

$$ET_{cp} = \frac{L1 + L2}{W\left(\frac{2}{K1} + \frac{1}{K2}\right)} \tag{B4}$$

where the subscript *cp* denotes the payload-face sheet composite, *W* the width of a detector (equal to *L2* for square detector segments), and *L1* and *L2* length dimensions as shown in Figure 12. Expressions B2 though B4 are applicable to the lower surface in the Y direction, for the upper surface the converter product (ET_c) is set to zero. Note that the segment simulation is appropriate for the entire panel width because the stiffness remains constant for each segment.

10.3 Composite ET in ladder direction (*X*)

The ladder composite equivalent *ET* is computed using the following expressions where *L3* is the gap distance filled by the detector bond material between detector segments.

$$K13 = \frac{1}{\frac{L3}{W} ET_{b\,\mathrm{det}} + \frac{2L1}{W} ET_d} \tag{B5}$$

$$K1 = \frac{W}{L1}\left(ET_{fsX} + ET_b + ET_c\right) \tag{B6}$$

$$K23 = \frac{1}{\frac{L3}{W}\left(ET_{fsX} + ET_b + 2ET_{bd}\right) + \frac{2}{K1}} \tag{B7}$$

$$K3 = K13 + K23 \tag{B8}$$

$$K2 = \frac{L1}{L2} K1 + K22 \tag{B9}$$

$$ET_{cp} = \frac{4L}{W}\left[\frac{1}{\frac{2}{K1} + \frac{4}{K3} + \frac{5}{K2}}\right] \tag{B10}$$

10.4 Payload modulus and density

The payload effective modulus is determined by

$$E_{pay} = \frac{ET_{cp} - ET_{fs}}{tk_{pay}} \tag{B11}$$

where the subscripts appearing in B11 are generic and represent the *X* or *Y* directions and the top or bottom composites as appropriate. Payload thickness tk_{pay} is taken as 10^{-6}m to ensure that the payload bending stiffness contribution is essentially zero (membrane stiffness only).

Payload density is calculated by the following expressions

$$M1 = W\ L\left(\rho_d tk_d + \rho_b tk_b + 2\rho_{bd} tk_{bd} + \rho_c tk_c\right) \tag{B12}$$

$$M_{cp} = W\ L2\left(M1 + \rho_{bd} tk_{bd}\right) \tag{B13}$$

$$\rho_{pay} = \frac{M_{cp}}{W\ L\ tk_{pay}} \tag{B14}$$

where the symbol ρ denotes density. Results for the baseline payload effective modulus and density are given in Table 14.

Payload	Standard GLAST		Super GLAST	
	Modulus (Pa)	Density (kg/m^3)	Modulus (Pa)	Density (kg/m^3)
Top X	2.805E13	1.626E6	2.805E13	1.625E6
Top Y	2.093E13		2.093E13	
Bottom X	3.055E13	3.894E6	4.491E13	17.50E6
Bottom Y	2.431E13		4.363E13	

Table 14: Calculated effective baseline payload modulus and density.

10.5 Poisson ratio determination

Given that there may be an orthotropic face sheet and that the payload models are clearly orthotropic, it is essential that an appropriate Poisson ratio is used in the payload FEM. A nominal value of Poisson ratio 0.3 is assigned and then the payload modulus in Y is compared with the modulus in X.

$$\nu = 0.3$$
$$if \quad E_{payY} \geq E_{payX} \tag{B15}$$
$$then \quad \nu = 0.3\frac{E_{payX}}{E_{payY}}$$